

Generalized first-principles method to study near-field heat transfer mediated by Coulomb interaction

Tao Zhu* and Jian-Sheng Wang

Department of Physics, National University of Singapore, Singapore 117551, Republic of Singapore

(Dated: June 15, 2022)

We present a first-principles approach to calculate the Coulomb-interaction-mediated heat current in the near field. With the nonequilibrium Green's functions method, the heat flux is calculated from a Landauer formula combining with a Caroli formula of transmission coefficient. The central physical quantities are the screened Coulomb potential and the spectrum function of polarizability. Within the random phase approximation, we calculate the polarizability using the linear response density functional theory and obtain the screened Coulomb potential from a retarded Dyson equation. We adopt single-layer graphene as an example to calculate the Coulomb heat flux between two parallel sheets with different gap sizes. Our results show that the heat flux saturates at the extreme near field with a convergent ratio of 5×10^4 to the black-body limit. With increasing distances, the heat flux asymptotically shows a $1/d^2$ dependence. From the energy current spectrum, we infer that the near-field enhancement of Coulomb heat flux stem from electron transitions around the Fermi level. Strain effects on the heat flux are also discussed at different distances. We found that the heat flux is positively correlated to the strain for most of the distances while a negative correlation is shown at the near-to-medium field. Our method is general and can be easily applied to various kinds of materials which provides a benchmarking reference for both theory and experiment.

From the 1970s, heat transfer in the near field has attracted extensive interest for its colossal thermal radiation over the black-body limit [1–3]. When the gap size is smaller than Wien's wavelength, experimental works reveal that the heat flux between two parallel plates can achieve thousands of times more than that being predicted by Stefan-Boltzmann law [4–6]. The most widely recognized theoretical explanation of such near-field effects is given by the fluctuational electrodynamics of Rytov [7, 8] with the further development of Poler and van Hove (PvH) [9]. In the PvH theory, the heat flux is generated by thermally driven current fluctuations that follow the equilibrium fluctuation-dissipation theorem [10, 11]. Based on macroscopic Maxwell's equations, the energy current is given by a Landauer-type expression with transmission coefficients that consist of contributions from both propagating and evanescent modes. The great enhancement of thermal radiation in the near field is due to the tunneling of evanescent waves that decay exponentially with the gap size [12, 13].

Recent experiments have approached distances down to the scale of nanometers to angstroms in which extraordinary large heat current have been found [14–17]. The reported near-field enhancements exceed the value predicted by the PvH theory and have been partially explained by mechanisms such as phonon tunneling or potential contaminants [18–20]. On the other hand, many efforts have been devoted to developing microscopic theories beyond the fluctuational electrodynamics and a scalar field theory of heat transfer has been proposed [21–24]. In the extreme near field, the vector potential of current fluctuations is less important and the scalar potential of density fluctuations becomes dominant [25].

In the quasi-static limit, the scalar potential gives rise to the instantaneous Coulomb interactions. Using the nonequilibrium Green's functions (NEGF) method, the transmission coefficient is given by a Caroli formula [26] with screened Coulomb potential and spectrum function of polarizability. It is equivalent to the formula obtained from the Joule heating effect of charge fluctuations due to external electric fields [27, 28] and agrees to the p-polarized evanescent modes without retardation effects [29, 30].

This Coulomb-type heat transfer has been studied for some systems [28, 29, 31–33]. However, specific theoretical modeling of density correlation functions is needed for different materials to obtain the transmission coefficient. In this letter, we introduce a generalized parameter-free first-principles method to calculate the Coulomb heat flux between two parallel plates. We follow the NEGF scheme of the scalar field theory and obtain the density correlation function from electronic band structures calculated from the density functional theory (DFT) [34]. This method can be easily applied to different materials with arbitrary thicknesses.

From the NEGF method, the energy current per unit area between two parallel plates is given by the Landauer formula

$$J = \frac{1}{A} \int_0^\infty \frac{d\omega}{2\pi} \hbar\omega [N_1(\omega) - N_2(\omega)] T(\omega), \quad (1)$$

where A is the area of plates and $N_\alpha = 1/(e^{\hbar\omega/(k_B T_\alpha)} - 1)$ is the Bose distribution function at the temperature T_α for plate α . In the local equilibrium approximation, Eq. (1) can be derived from the Meir-Wingreen formula [35, 36] and the transmission coefficient $T(\omega)$ is given by a Caroli formula [26, 29]

$$T(\omega) = \text{Tr}[D^r \Gamma_1 D^a \Gamma_2], \quad (2)$$

* phyzht@nus.edu.sg

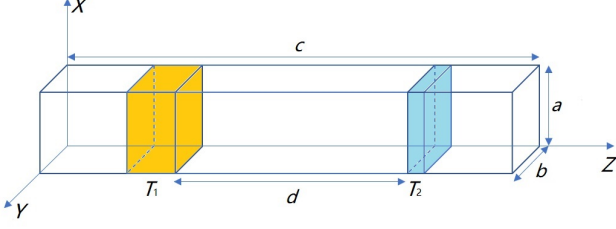


FIG. 1. Sketch of unit simulation box of two parallel plates with a vacuum gap of d . Each of the plates is in its own internal thermal equilibrium state, i.e. plate 1 has temperature T_1 and plate 2 has temperature T_2 . a , b , and c are lattice constant along x , y , and z direction, respectively.

where superscripts r and a denote retarded and advanced component, respectively. The screened Coulomb potential D follows the Dyson equation [37] $D = D^0 + D^0 \Pi D$ for the scalar-field Green's function. At the quasi-static limit, D^0 has only the component of pure Coulomb potential v . In real space, we can write the retarded Dyson equation as

$$D^r(\mathbf{r}, \mathbf{r}', \omega) = v(\mathbf{r}, \mathbf{r}') + \int d\mathbf{r}'' \int d\mathbf{r}''' v(\mathbf{r}, \mathbf{r}'') \times \Pi^r(\mathbf{r}'', \mathbf{r}''', \omega) D^r(\mathbf{r}''', \mathbf{r}', \omega), \quad (3)$$

where Π^r is the retarded scalar photon self-energy or the polarizability that represents the linear response of the induced charge density to the total potential of the system. Within the random phase approximation (RPA) [38], the linear-response Kubo's formalism of polarizability writes [39, 40]

$$\Pi^r(\mathbf{r}, \mathbf{r}', \omega) = 2e^2 \sum_{i,j} (f_j - f_i) \frac{\psi_j(\mathbf{r}) \psi_j^*(\mathbf{r}') \psi_i^*(\mathbf{r}) \psi_i(\mathbf{r}')}{\epsilon_j - \epsilon_i - \hbar\omega - i\eta}, \quad (4)$$

where $\psi_{i(j)}$ and $\epsilon_{i(j)}$ are volume-normalized independent particle wave-functions and energies of state i (j), respectively. The function $f = (1 + e^{\beta(\epsilon - \mu)})^{-1}$ is the Fermi distribution function with $\beta = 1/k_B T$ and μ the chemical potential. The factor 2 accounts for the spin degeneracy and e is the electron charge. The damping factor η is a small positive quantity that accounts for the carrier relaxation of long-range scatterers [41].

In Eq. (2), the spectrum function of each plate is defined as $\Gamma_\alpha = i(\Pi_\alpha^r - \Pi_\alpha^a)$ with $\alpha = 1$ or 2 and Π_α is the individual polarizability of plate α in isolation. As the advanced components are the Hermitian transpose of the retarded one, i.e. $D^a = (D^r)^\dagger$ and $\Pi^a = (\Pi^r)^\dagger$, in the following discussion, we omit the superscript and all quantities are retarded unless otherwise specified.

With Eqs. (1) to (4), one can obtain the heat flux between two parallel plates with arbitrary thickness. However, both polarizability Π and screened Coulomb poten-

tial D are difficult to solve in real space as the position \mathbf{r} is continuous. For periodic systems, due to translational invariance $f(\mathbf{r} + \mathbf{R}, \mathbf{r}' + \mathbf{R}) = f(\mathbf{r}, \mathbf{r}')$, it is more convenient to calculate these quantities in momentum space with the Bloch wave vector \mathbf{q} and the reciprocal lattice vector \mathbf{G} .

We show in Fig. 1 the unit simulation box of two parallel plates separated by a vacuum gap of d . From the Dyson equation, the screened Coulomb potential can be written as $D = \epsilon^{-1}v$ where ϵ is the dielectric function that is given by

$$\epsilon_{\mathbf{G}, \mathbf{G}'}(\mathbf{q}, \omega) = \delta_{\mathbf{G}, \mathbf{G}'} - v_{\mathbf{G}, \mathbf{G}'}(\mathbf{q}) \Pi_{\mathbf{G}, \mathbf{G}'}(\mathbf{q}, \omega). \quad (5)$$

The Fourier transform of the pure Coulomb potential in the momentum space is

$$v_{\mathbf{G}, \mathbf{G}'}(\mathbf{q}) = \delta_{\mathbf{G}, \mathbf{G}'} \frac{1}{\epsilon_0 |\mathbf{q} + \mathbf{G}|^2}, \quad (6)$$

where $\epsilon_0 \approx 8.85 \times 10^{-12}$ F/m is the vacuum permittivity.

In RPA, the polarizability can be obtained from DFT with the Adler-Wiser formula [42, 43]

$$\Pi_{\mathbf{G}, \mathbf{G}'}(\mathbf{q}, \omega) = \frac{2e^2}{\Omega} \sum_{n, n', \mathbf{k}} w_{\mathbf{k}} (f_{n'\mathbf{k}+\mathbf{q}} - f_{n\mathbf{k}}) \times \frac{\langle \phi_{n\mathbf{k}} | e^{-i(\mathbf{q}+\mathbf{G}) \cdot \mathbf{r}} | \phi_{n'\mathbf{k}+\mathbf{q}} \rangle \langle \phi_{n'\mathbf{k}+\mathbf{q}} | e^{i(\mathbf{q}+\mathbf{G}') \cdot \mathbf{r}} | \phi_{n\mathbf{k}} \rangle}{\epsilon_{n'\mathbf{k}+\mathbf{q}} - \epsilon_{n\mathbf{k}} - \hbar\omega - i\eta}, \quad (7)$$

where $\phi_{n\mathbf{k}}$ and $\epsilon_{n\mathbf{k}}$ are Kohn-Sham [44] eigenfunctions and eigenvalues, respectively. The Fermi occupation function f equals 1 for occupied states and 0 for unoccupied states. Ω is the volume of the primitive cell and $w_{\mathbf{k}}$ is the weight of each k -point in the first Brillouin zone which accounts for symmetry.

With Eqs. (5) to (7), one can calculate the heat flux from the Landauer formula Eq. (1) with the transmission coefficient

$$T(\omega) = \sum_{\mathbf{q}} \text{Tr}_{\mathbf{G}} [D \Gamma_1 D^\dagger \Gamma_2], \quad (8)$$

where \mathbf{q} lies in the first Brillouin zone. All quantities inside the bracket of Eq. (8) involve matrix multiplications with dimensions of $N \times N$ where N is the number of \mathbf{G} vectors which is subject to the kinetic energy cutoff of response functions, i.e. $|\mathbf{q} + \mathbf{G}|^2 < E_{\text{cut}}$. The trace is only applied to the \mathbf{G} space.

Because two plates are localized in the z -direction with a vacuum gap of d , a sufficiently large number of G_z components may be required. If there is no electronic tunneling between two plates, i.e., the Hamiltonian is block diagonal, the polarizability of the system can be written as $\Pi = \Pi_1 + \Pi_2$ which in the \mathbf{G} space writes

$$\Pi = \begin{pmatrix} \Pi_{11} & 0 \\ 0 & \Pi_{22} \end{pmatrix}, \quad (9)$$

where Π_{11} and Π_{22} are submatrix of Π_1 and Π_2 with dimensions of $N_1 \times N_1$ and $N_2 \times N_2$, respectively. In other

words, each diagonal block of the whole polarizability matrix consists of localized polarizability of each plate in isolation and all entries in the off-diagonal block are zero. In this case, we can simplify our problem by separating the whole system into two independent pieces and do separate calculations of Π_1 and Π_2 with the same unit cell and same sets of \mathbf{G} vectors [45].

Moreover, if both of two plates are two-dimensional (2D) materials that electrons are confined in the plane perpendicular to the z -axis, i.e. $\rho(\mathbf{r}_\perp, z) \propto \delta(z)$. We can further simplify the problem by introducing the 2D surface density

$$\sigma(\mathbf{r}_\perp) = \int_{-\infty}^{\infty} \rho(\mathbf{r}_\perp, z) dz \quad (10)$$

into the Kubo's formalism and derive the 2D polarizability as [46]

$$\Pi_{\mathbf{G}_\perp, \mathbf{G}'_\perp}^{2D}(\mathbf{q}_\perp, \omega) = c \times \Pi_{(\mathbf{G}_\perp, 0), (\mathbf{G}'_\perp, 0)}^{3D}((\mathbf{q}_\perp, 0), \omega), \quad (11)$$

where c is the lattice constant in z direction. Eq. (11) implies that we can reduce the original three-dimensional (3D) problem to a 2D problem by sampling \mathbf{q} and \mathbf{G} with only in-plane components, i.e. $(\mathbf{q}_\perp, 0)$ and $(\mathbf{G}_\perp, 0)$. Without cross correlation between two sides, the Dyson equation of Eq. (3) has a matrix form

$$\begin{pmatrix} \varepsilon_1 & -v_{12}\Pi_{22} \\ -v_{21}\Pi_{11} & \varepsilon_2 \end{pmatrix} \begin{pmatrix} D_{11} & D_{12} \\ D_{21} & D_{22} \end{pmatrix} = \begin{pmatrix} v_{11} & v_{12} \\ v_{21} & v_{22} \end{pmatrix}, \quad (12)$$

where $\varepsilon_\alpha = I - v_{\alpha\alpha}\Pi_{\alpha\alpha}$ is the dielectric function of plate α . The components of 2D pure Coulomb potential is defined as

$$[v_{\alpha\beta}]_{\mathbf{G}, \mathbf{G}'} = \delta_{\mathbf{G}, \mathbf{G}'} \frac{e^{-|\mathbf{q} + \mathbf{G}| |z_\alpha - z_\beta|}}{2\varepsilon_0 |\mathbf{q} + \mathbf{G}|}, \quad (13)$$

where $z_{\alpha(\beta)}$ is the coordinate of plate α (β) in the z -axis. Taking the trace of each side explicitly, the transmission function in Eq. (8) can be simplified as

$$T(\omega) = \sum_{\mathbf{q}} \text{Tr}_{\mathbf{G}} [D_{12} \Gamma_{11} D_{21}^\dagger \Gamma_{22}], \quad (14)$$

where all quantities are in the 2D form and \mathbf{q} lies in the 2D first Brillouin zone.

It is worthwhile to mention that Eq. (8) is valid for both 2D and 3D problems provided that all quantities are consistent in dimension. However, the computational cost is significantly reduced for the 2D cases with Eqs. (11) to (14). As an example, we calculate the heat flux between two parallel single-layer graphene sheets. Similar procedures can be applied to other materials with arbitrary thickness.

We start from the ground state calculations by using density functional theory as implemented in QUANTUM ESPRESSO [47, 48]. We adopt the norm-conserving pseudopotential generated by the Martins-Troullier method [49] with the Perdew-Burke-Ernzerhof

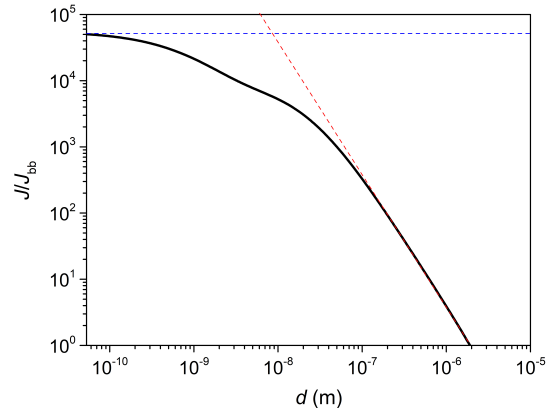


FIG. 2. Calculated heat flux ratio between two parallel graphene sheets with different gap sizes. The blue dashed line represents the saturation trend of the heat flux at small distances. The red dashed line has a slope of -2 that shows the asymptotic $1/d^2$ dependence of the heat flux at large distances.

exchange-correlation functional [50] in the generalized gradient approximation. The plane-wave basis set with 60 Ry energy cut-off is used to expand the Kohn-Sham wave functions. The Fermi-Dirac smearing with 0.002 Ry smearing width has been employed to treat the partial occupancies. The in-plane lattice constant are $a = b = 2.46 \text{ \AA}$. To avoid interactions from the neighboring lattice in the z direction, a large lattice constant of $c = 18 \text{ \AA}$ is set in z direction of the unit cell.

The polarizability of each side is calculated on top of the ground state band structure by using the BerkeleyGW package [51, 52]. A $90 \times 90 \times 1$ Monkhorst-Pack [53] grid is used to sample the first Brillouin zone for the nonlocal polarizability while the long-wave ($q \rightarrow 0$) polarizability is obtained from a $300 \times 300 \times 1$ grid. To avoid divergence of the Coulomb potential, we use a small value of $q = 10^{-5}$ a.u. in the calculation of contributions from the long-wave polarizability. The energy broadening factor η is set to 0.05 eV that corresponds to an electron relaxation time of 10^{-14} s [54]. We also neglect the local field effects [55] that are only important for systems with inhomogeneous geometry [34, 56], i.e. only $\mathbf{G} = 0$ used. Then we solve the Dyson equation to get the screened Coulomb potential and calculate the transmission coefficient from the Caroli formula. At last, we integrate over frequencies to get the heat flux.

In Fig. 2, we show the calculated heat flux of two parallel graphene sheets with different gap sizes. The temperature is fixed at $T_1 = 1000$ K and $T_2 = 300$ K. The vertical coordinate is the ratio of the Coulomb heat flux calculated from our method to the black-body radiative heat flux given by the Stefan-Boltzmann law $J_{bb} = \sigma(T_1^4 - T_2^4)$ with $\sigma \approx 5.67 \times 10^{-8} \text{ W}/(\text{m}^2\text{K}^4)$. As seen, the Coulomb interaction mediated heat current is remarkably larger than that of the black-body radiation. At small dis-

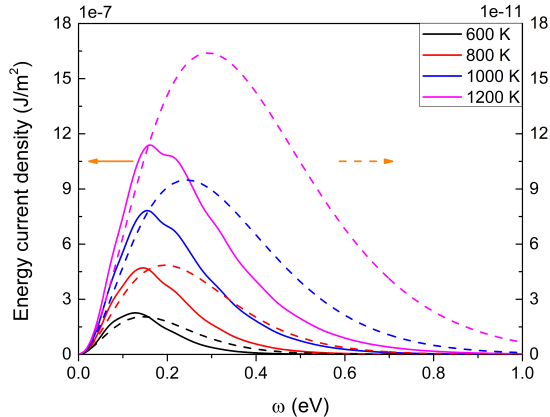


FIG. 3. The Coulomb (solid curve, left axis) and black-body radiative (dashed curve, right axis) energy current density of graphene with different temperatures. The distance is fixed at $d = 100$ nm. The left and right axis share the same scale of ticks but differ by 4 orders of magnitude.

tances, the heat flux ratio has a convergent value around 5×10^4 that agrees with the previous report [31]. The saturation of heat flux at the extreme near field originates from the nonlocal effect of wave vectors, which agree with the behavior of thermal radiation mediated by p-polarized evanescent waves [57]. With an increase of distances, the heat flux decrease monotonically. Due to the exponential factor that appears in the 2D Coulomb potential, the long-wave ($q \rightarrow 0$) contribution becomes dominant at large distances. When $d > 100$ nm, the heat flux shows an asymptotic dependence of $1/d^2$ which is consistent with Coulomb's law. When $d > 2 \mu\text{m}$, the Coulomb heat flux is smaller than that of the black-body radiation. This agrees with the fact that heat transfer is mainly achieved by propagating waves in the far-field [12]. With a further increase of the distance, the retardation effects can not be ignored and our theory breaks down.

Figure 3 shows the comparison of Coulomb and black-body radiative energy current density of graphene with different temperatures. The black-body energy current density is given by Planck's law and only depends on frequency and temperature. On the other hand, as shown in Eq. (13), the Coulomb interaction decay exponentially with the gap sizes. In our calculation, we fixed the distance at $d = 100$ nm where non-local effects become less significant. As can be seen, the Coulomb energy current density is approximately 4 orders of magnitude larger than that of black-body radiation. Moreover, most spectrum weights of Coulomb energy current density lie in the low frequencies while the black-body radiation has a broader spectrum. When $\omega < 0.16$ eV, the Coulomb energy current density has a similar increasing trend as the black-body spectrum. However, with a further increase of frequency, the Coulomb energy current density decay rapidly and vanish at high frequencies. This im-

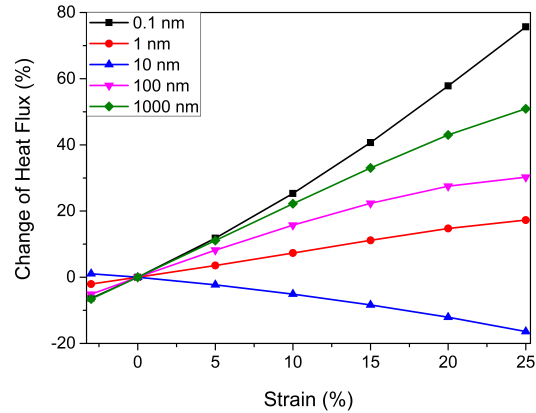


FIG. 4. Strain effect on the Coulomb heat flux between two parallel single-layer graphene sheets with different gap sizes. The horizontal axis is the magnitude of strain in percentage and vertical axis is the percentage change of heat flux after strain is applied.

plies that the near-field enhancement of Coulomb energy current between two graphene sheets is mainly attributed to electron transitions around the Fermi level.

Another advantage of our method is that one can easily change the parameters of materials without theoretical treatment on models. Experimentally, strains arise naturally in graphene due to the surface corrugations [58] or lattice mismatch [59] between graphene and substrate. In Fig. 4, we show the strain effect on the heat flux between two graphene sheets with different gap sizes. We introduce the uniform biaxial strain by varying the lattice constant with a percentage change from -3% to 25% and calculate the heat flux after strain is applied. As shown in Fig. 4, the heat flux is positively correlated to the strain for most of the gap size. For example, at $d = 0.1$ nm, the calculated heat flux increases up to 75% with a 25% strain. This enhancement may originate from effective electronic scalar potential induced by uniform strain in graphene [60, 61]. Interestingly, with an increase of gap size, the enhancement becomes less significant at $d = 1$ nm and even a negative dependence is shown at $d = 10$ nm. This would due to the interplay between local and nonlocal effects in calculating the transmission coefficient in the near-to-medium field. With further increase of the gap size, the long-wave component dominate, and the heat fluxes again show a positive correlation to the strain applied.

In summary, we have presented a general first-principles method to study the near-field heat transfer mediated by Coulomb interaction. The heat flux is calculated from a Landauer formula with a transmission coefficient that is given by a Caroli formula. Within the density functional theory, we calculate the polarizability from electronic band structures and obtain the screened Coulomb interaction with the retarded Dyson equation. We adopted single-layer graphene as an example to cal-

culate the heat flux between two parallel sheets. Our results show that the Coulomb heat flux is significantly larger than that of the black-body radiation at small distances. With an increase of gap sizes, an asymptotic dependence of $1/d^2$ is shown. The spectrum weight of Coulomb energy current concentrates at low frequencies which implies that the near-field enhancement originates from electron transitions around the Fermi level. For most of the gap sizes, the calculated heat flux has a

positive correlation with the strain applied. A negative correlation is shown in the near-to-medium field which may originate from the interplay between local and non-local effects. Our method can be used to study Coulomb heat transfer of a wide range of materials that provides a benchmarking reference for both theory and experiment.

Acknowledgments. This work is supported by FRC grant R-144-000-427-114 and MOE tier 2 grant R-144-000-411-112.

-
- [1] A. I. Volokitin and B. N. J. Persson, *Rev. Mod. Phys.* **79**, 1291 (2007).
- [2] Z. M. Zhang, *Nano/Microscale Heat Transfer* (Springer, Cham Switzerland, 2020).
- [3] S.-A. Biehs, R. Messina, P. S. Venkataram, A. W. Rodriguez, J. C. Cuevas, P. Ben-Abdallah, arXiv:2007.05604.
- [4] C. M. Hargreaves, *Phys. Lett. A* **30**, 491 (1969).
- [5] G. A. Domoto, R. F. Boehm, and C. L. Tien, *J. Heat Transfer*. **92**(3), 412 (1970).
- [6] R. S. Ottens, V. Quetschke, S. Wise, A. A. Alemi, R. Lundock, G. Mueller, D. H. Reitze, D. B. Tanner, and B. F. Whiting, *Phys. Rev. Lett.* **107** 014301 (2011).
- [7] S. M. Rytov, *Theory of electric fluctuations and thermal radiation* (Air Force Cambridge Research Center, Bedford, MA, 1953).
- [8] S. M. Rytov, Y. A. Kravtsov, and V. I. Tatarskii, *Principles of statistical radiophysics* (Springer-Verlag, Berlin Heidelberg, 1989).
- [9] D. Polder and M. A. van Hove, *Phys. Rev. B* **4**, 3303 (1971).
- [10] H. Nyquist, *Phys. Rev.* **32** 110 (1928).
- [11] H. B. Callen and T. A. Welton, *Phys. Rev.* **83** 34 (1951).
- [12] B. Song, A. Fiorino, E. Meyhofer, and P. Reddy, *AIP Adv.* **5**, 053503 (2015).
- [13] J. C. Cuevas, and F. J. García-Vidal, *ACS Photonics* **5**, 3896 (2018).
- [14] A. Kittel, W. Müller-Hirsch, J. Parisi, S.-A. Biehs, D. Reddig, and M. Holthaus, *Phys. Rev. Lett.* **95**, 224301 (2005).
- [15] I. Altfeder, A. A. Voevodin, and A. K. Roy, *Phys. Rev. Lett.* **105**, 166101 (2010).
- [16] K. Kloppstech, N. Köhne, S.-A. Biehs, A. W. Rodriguez, L. Worbes, D. Hellmann, and A. Kittel, *Nat. Commun.* **8**, 14475 (2017).
- [17] L. Worbes, D. Hellmann, and A. Kittel, *Phys. Rev. Lett.* **110**, 134302 (2013).
- [18] V. Chiloyan, J. Garg, K. Esfarjani and G. Chen, *Nat. Commun.* **6**, 6755 (2015).
- [19] S. Xiong, K. Yang, Y. A. Kosevich, Y. Chalopin, R. D'Agosta, P. Cortona, and S. Volz, *Phys. Rev. Lett.* **112**, 114301 (2014).
- [20] L. Cui, W. Jeong, V. Fernández-Hurtado, J. Feist, F. J. García-Vidal, J. C. Cuevas, E. Meyhofer, and P. Reddy, *Nat. Commun.* **8**, 14479 (2017).
- [21] J.-S. Wang and J. Peng, arXiv:1607.02840.
- [22] J.-S. Wang and J. Peng, *EPL*, **118** 24001 (2017).
- [23] J. Peng, H. H. Yap, G. Zhang, and J.-S. Wang, arXiv:1703.07113.
- [24] G. Tang and J.-S. Wang, *Phys. Rev. B* **98**, 125401 (2018).
- [25] G. D. Mahan, *Phys. Rev. B* **95**, 115427 (2017).
- [26] C. Caroli, R. Combescot, P. Nozieres, and D. Saint-James, *J. Phys. C* **4**, 916 (1971).
- [27] J.-S. Wang, Z.-Q. Zhang, and J. T. Lü, *Phys. Rev. E* **98**, 012118 (2018).
- [28] R. Yu, A. Manjavacas, and F. J. García de Abajo, *Nat. Commun.* **8**, 2 (2017).
- [29] Z.-Q. Zhang, J. T. Lü, and J. -S. Wang, *Phys. Rev. B* **97**, 195450 (2018).
- [30] T. Zhu, Z.-Q. Zhang, Z. Gao, and J.-S. Wang, *Phys. Rev. Appl.* **14** 024080 (2020).
- [31] J.-H. Jiang, and J.-S. Wang, *Phys. Rev. B* **96**, 155437 (2017).
- [32] G. Tang, H. H. Yap, J. Ren, and J.-S. Wang, *Phys. Rev. Applied* **11**, 031004 (2019).
- [33] K. N. Lian and J.-S. Wang, *Eur. Phys. J. B* **93**, 138 (2020).
- [34] G. Onida, L. Reining, and A. Rubio, *Rev. Mod. Phys.* **74**, 601 (2002).
- [35] Y. Meir and N. S. Wingreen, *Phys. Rev. Lett.* **68**, 2512 (1992).
- [36] A.-P. Jauho, N. S. Wingreen, and Y. Meir, *Phys. Rev. B* **50**, 5528 (1994).
- [37] F. J. Dyson, *Phys. Rev.* **75**, 1736 (1949).
- [38] H. Ehrenreich, and M. H. Cohen, *Phys. Rev.* **115**, 786 (1959).
- [39] R. Kubo, *J. Phys. Soc. Jpn.* **12**, 570 (1957); R. Kubo, M. Yokota, and S. Nakajima, *ibid.* **12**, 1203 (1957).
- [40] T. Zhu, M. Antezza and J.-S. Wang, *Phys. Rev. B* **103**, 125421 (2021).
- [41] N. D. Mermin, *Phys. Rev. B* **1**, 2362 (1970).
- [42] S. L. Adler, *Phys. Rev.* **126**, 413 (1962).
- [43] N. Wiser, *Phys. Rev.* **129**, 62 (1963).
- [44] W. Kohn, and L. Sham, *Phys. Rev.* **140**, A1133 (1965).
- [45] F. Xuan, Y. Chen, and S. Y. Quek, *J. Chem. Theory Comput.* **15**, 3824 (2019).
- [46] F. A. Rasmussen, Doctor of Philosophy, Technical University of Denmark (2016).
- [47] P. Giannozzi, S. Baroni, N. Bonini, M. Calandra, R. Car, C. Cavazzoni, D. Ceresoli, G. L. Chiarotti, M. Cococcioni, I. Dabo *et al.*, *J. Phys.:Condens.Matter* **21**, 395502 (2009).
- [48] P. Giannozzi, O. Andreussi, T. Brumme, O. Bunau, M. B. Nardelli, M. Calandra, R. Car, C. Cavazzoni, D. Ceresoli, M. Cococcioni *et al.*, *J. Phys.:Condens.Matter* **29**, 465901 (2017).
- [49] N. Troullier and J. L. Martins, *Phys. Rev. B* **43**, 1993 (1991).

- [50] J. P. Perdew, K. Burke, and M. Ernzerhof, Phys. Rev. Lett. **77**, 3865 (1996).
- [51] M. S. Hybertsen and S. G. Louie, Phys. Rev. B **34**, 5390 (1986).
- [52] J. Deslippe, G. Samsonidze, D. A. Strubbe, M. Jain, M. L. Cohen, and S. G. Louie, Comput. Phys. Commun. **183**, 1269 (2012).
- [53] H. J. Monkhorst, and J. D. Pack, Phys. Rev. B **13**, 5188 (1976).
- [54] O. Ilic, M. Jablan, J. D. Joannopoulos, I. Celanovic, H. Buljan, and M. Soljačić, Phys. Rev. B **85**, 155422 (2012).
- [55] S. G. Louie, J. R. Chelikowsky, and M. L. Cohen, Phys. Rev. Lett. **34**, 155 (1975).
- [56] T. Zhu, P. E. Trevisanutto, T. C. Asmara, L. Xu, Y. P. Feng, and A. Rusydi, Phys. Rev. B **98**, 235115 (2018).
- [57] P. -O. Chapuis, S. Volz, C. Henkel, K. Joulain, and J. -J. Greffet, Phys. Rev. B **77**, 035431 (2008).
- [58] M. Teague, A. Lai, J. Velasco, C. Hughes, A. Beyer, M. Bockrath, C. Lau and N.-C. Yeh, Nano Lett. **9**, 2542 (2009).
- [59] Z. Ni, W. Chen, X. Fan, J. Kuo, T. Yu, A. Wee and Z. Shen, Phys. Rev. B **77**, 115416 (2008).
- [60] S.-M. Choi, S.-H. Jhi, and Y.-W. Son, Phys. Rev. B **81**, 081407(R) (2010).
- [61] C. Si, Z. Sun, and F. Liu, Nanoscale **8**, 3207 (2016).